Efficient and Accurate Sampling of the Thermal Neutron Scattering Law in OpenMC

by

Amelia J. Trainer

SUBMITTED TO THE DEPARTMENT OF NUCLEAR SCIENCE AND ENGINEERING IN PARTIAL FULFILLMENT OF THE REQUIREMENTS FOR THE DEGREE OF

MASTER OF SCIENCE IN NUCLEAR SCIENCE AND ENGINEERING

AT THE

MASSACHUSETTS INSTITUTE OF TECHNOLOGY

JUNE 2019

Signature of Author:⎽⎽

Amelia J. Trainer
Department of Nuclear Science and Engineering
May 18, 2019

Certified by:⎽⎽⎽

Benoit Forget
Associate Professor of Nuclear Science and Engineering
Thesis Supervisor

Accepted by:⎽⎽⎽

Michael Short
Assistant Professor of Nuclear Science and Engineering
Chairman, NSE Committee for Undergraduate Students

Efficient and Accurate Sampling of the Thermal Neutron Scattering Law in OpenMC

by

Amelia J. Trainer

Submitted to the Department of Nuclear Science
and Engineering on May 18, 2019 in Partial
Fulfillment of the Requirements for the Degree of
Master of Science in Nuclear Science and
Engineering

ABSTRACT

THIS IS MY ABSTRACT LOCATED IN TITLEPAGE.TEX

Thesis Supervisor: Benoit Forget
Title: Associate Professor of Nuclear Science and Engineering

Thesis Reader: Kord Smith
Title: Korea Electric Power Company (KEPCO) Professor of the Practice of Nuclear Science and Engineering

Acknowledgements

Thanks

Contents

List of Figures

List of Tables

Chapter 1

Introduction

1.1 Motivation

The merit of a nuclear system simulation is heavily dependent on the accuracy of the input nuclear data. Nuclear data (such as cross sections, particle emissions, etc.) is often complicated and highly energy dependent, which poses a challenge for those interested in effcieiently simulating the behavior of a nuclear system. Nuclear data is released in "evaluations", which are prepared by statistically combining experimentally measured data with theoretical predictions. The most widely used format for these evaluations is called the Evaluated Nuclear Data File (ENDF) [1]. ENDF files are generally not directly used by nuclear simulations, but are rather preprocessed to account for simulation-specific conditions. In doing so, the ENDF is converted into a more usable form, called "a compact ENDF" (ACE) [2].

Currently, the most widely trusted code used for nuclear data preprocessing is NJOY, which has been developed and maintained at Los Alamos National Lab (LANL) since the early 1970's [3]. It has a large users base and is versatile for many nuclear data related tasks, including resonance reconstruction, Doppler-Broadening, multi-group cross section generation, and the preparation of thermal neutron scattering data. NJOY's capabilities are spread across 24 modules, each of which has a specified task. Two modules in particular, LEAPR and THERMR, handle the calculation and representation of thermal scattering from bound moderators. While the accuracy of thermal neutron scattering data can greatly dictate the quality of thermal reactor analysis and safety margin calculations, it remains a difficult problem, due to effects (molecular structure, neutron wavelength, described below) that are not apparent for higher neutron energies.

Both thermal neutron scattering and resonant neutron scattering are highly dependent on incoming neutron energy. However, thermal neutron scattering cross sections must also account for molecular structure, since the energy of the incoming neutron is generally on the order of the molecules' excitation modes (i.e. below 1-10 eV). Excitation of these excitation modes can result in vibration, translation, or rotation of the target. Vibrational modes, also called phonons, are a primary concern when describing neutron scattering in a solid. In addition to the molecular excitation, thermal neutrons data processing is further complicated by considering the long neutron de Broglie wavelength. When

a neutron has energy in the thermal region, its wavelength can be on the order of the interatomic spacing, which allows it to interact with multiple nuclei, as opposed to a single atom [4].

Despite the above complications, a thermal scattering relationship $S(\alpha, \beta, T)$ is constructed to relate unitless neutron momentum and energy exchange (α and β, respectively) with the double differential inelastic incoherent scattering cross section $\sigma(E \rightarrow E', \mu)$. Once $S(\alpha, \beta, T)$, also called the "scattering law", is obtained, the cross section can be obtained using

$$\sigma(E \rightarrow E', \mu) = \frac{\sigma_b}{2k_bT}\sqrt{\frac{E'}{E}}S(\alpha, \beta, T), \tag{1.1}$$

where σ_b is the characteristic bound scattering cross section of the target isotope, and k_b is Boltzmann's constant and T is the temperature. As shown in Eq. 1.1, if $S(\alpha, \beta, T)$ can be accurately obtained, the differential inelastic incoherent scattering cross section $\sigma(E \rightarrow E', \mu)$ is simple to calculate. Thus, the quality of thermal nuclear system modeling is directly tied to the preparation of the scattering law.

1.2 Current Methods of Preparing $S(\alpha, \beta, T)$

1.2.1 Types of Thermal Neutron Scattering

As mentioned in Sec. 1.1, the most widely used code for nuclear data processing is NJOY, which through two of its modules (LEAPR and THERMR) has the ability to prepare thermal scattering data. In particular, LEAPR is used to create a $S(\alpha, \beta, T)$ table, while THERMR tabulates the scattering law into a convenient form for simulations to use. Since LEAPR primarily calculates $S(\alpha, \beta, T)$, it will be of primary focus for the rest of this section.

Thermal neutron scattering can be broken into elastic and inelastic parts, which can then be further separated into coherent and incoherent parts. Elastic thermal scattering implies no change in neutron energy. Note that this differs from elastic scattering off of a single particle, in that a thermal neutron will elastically scatter off of an entire lattice, which makes the effective mass of the target extremely large. Thermal inelastic scattering can result in neutron energy loss, which corresponds to target excitation. At these low energies, neutron up-scattering can also occur, which implies neutron energy gain, and corresponds to target de-excitation. Excitations can correspond to creation of vibrational modes (phonons), as well as the creation of translational or rotational modes. For a system of particles with randomly distributed spins, coherent scattering consists of interacting wave effects, whereas incoherent scattering consists solely of a sum of non-interacting waves[1].

For materials with randomly distributed crystallites, the form of coherent inelastic scattering nearly equals that of incoherent inelastic scattering. This allows the coherent and incoherent inelastic components to be combined into one inelastic contribution, an

---

[1]Materials such as cold hydrogen that do not have randomly distributed have additional effects, so they have be considered apart from this simple coherent/incoherent discussion.

approximation known as the "incoherent approximation" [3, 4]. Thus, LEAPR separates the scattering calculation into inelastic, coherent elastic, and incoherent inelastic. This project focuses on inelastic scattering, due to the predominant importance of neutron energy change.

1.2.2 Inelastic Thermal Neutron Scattering

Recall from Sec. 1.1 that the double differential inelastic cross section is defined as

$$\sigma\left(E \to E', \mu\right) = \frac{\sigma_b}{2kT}\sqrt{\frac{E'}{E}} S_{n.sym}(\alpha, \beta, T) \tag{1.1}$$

which describes a neutron with incoming energy E scattering with cosine μ into energy E'. Recall again that σ_b is the characteristic bound scattering cross section for the target, k_b is Boltzmann's constant, and T is the temperature. Note that $S_{n.sym}(\alpha, \beta, T)$ is the non-symmetric form of the scattering law, which will be further discussed in !!!!!!!!!!!!!!!!!!!!!. Dimensionless momentum and energy transfer, α and β respectively, are defined as

$$\alpha = \frac{E' + E - 2\mu\sqrt{E'E}}{AkT} \tag{1.2}$$

$$\beta = \frac{E' - E}{kT} \tag{1.3}$$

The symmetric scattering law $S_{n.sym}(\alpha, \beta)$ can be written as an integral across time in units of $\hbar/k_bT$ seconds, [THIS USES THE GAUSSIAN APPROXIMATION SO CHECK OUT Scattering of Slow Neutrons by a Liquid George H. Vineyard]

$$S_{n.sym}(\alpha, \beta, T) = \frac{1}{2\pi}\int_{-\infty}^{\infty} e^{i\beta\hat{t}} e^{-\gamma(\hat{t})} \, d\hat{t} \tag{1.4}$$

where

$$\gamma(\hat{t}) = \alpha \int_{-\infty}^{\infty} P(\beta)\left[1 - e^{-i\beta\hat{t}}\right] e^{-\beta/2} \, d\beta \tag{1.5}$$

and

$$P(\beta) = \frac{\rho(\beta)}{2\beta\sinh(\beta/2)}. \tag{1.6}$$

Note that $\rho(\beta)$ is the phonon distribution or excitation frequency spectrum characteristic to the material, and that it normalizes to unity,

$$\int_{0}^{\infty} \rho(\beta)d\beta = 1. \tag{1.7}$$

Note that to get to this point, the only assumption made is that equating the form of incoherent inelastic scattering with that of coherent elastic scattering (incoheren approximation). At this point, LEAPR decomposes the frequency spectrum $\rho(\beta)$,

$$\rho(\beta) = \sum_{j=1}^{\# \text{ osc.}} \omega_j\delta(\beta_j) + \rho_s(\beta) + \rho_t(\beta)) \tag{1.8}$$

11

into a sum of discrete oscillators (represented by weighted delta-functions $\omega_j \delta(\beta_j)$), a solid-type spectrum $\rho_s(\beta)$, and a translational spectrum $\rho_t(\beta)$. The solid-type spectrum and translational spectrum integrate to ω_s and ω_t, respectively, such that

$$\sum_{j=1}^{\#\text{ osc.}} \omega_j + \omega_s + \omega_t = 1. \tag{1.9}$$

LEAPR uses each component of this decomposed frequency distribution to create a corresponding scattering law $S_{sym,i}(\alpha, \beta, T)$, then convolves these individual scattering laws to retreive the true scattering relation $S_{n.sym}(\alpha, \beta, T)$.

Solid-Type Continuous Spectra

The solid-type continuous conribution to $S_{n.sym}(\alpha, \beta, T)$, denoted with an (s) superscript, can be calculated by representing Eq. 1.4 as a sum, and using a finite number of terms of that sum to approximate a contribution value. The solid-type continuous spectra depends on the frequency distributino $\rho(\beta)$. Eq. 1.5 can be rewritten as

$$\gamma(\hat{t}) = \alpha \lambda_s - \alpha \int_{-\infty}^{\infty} P(\beta) e^{-\beta/2} e^{-i\beta \hat{t}} \, d\beta. \tag{1.10}$$

where λ_s, known as the Debye-Waller coefficient for the solid-type spectra, is defined as

$$\lambda_s = \int_{-\infty}^{\infty} P(\beta') e^{-\beta'/2} \, d\beta'. \tag{1.11}$$

Thus, the exponential of Eq. 1.10 is

$$e^{-\gamma(\hat{t})} = \sum_{n=0}^{\infty} \left(e^{-\alpha \lambda_s} \frac{1}{n!} \left[\alpha \int_{-\infty}^{\infty} P(\beta') e^{-\beta'/2} e^{-i\beta' \hat{t}} \, d\beta' \right]^n \right) \tag{1.12}$$

where the exponential of the latter term has been represented as a Taylor series. The above can be used in Eq. 1.4, yielding

$$S_{n.sym}^{(s)}(\alpha, \beta, T) = \frac{1}{2\pi} \int_{-\infty}^{\infty} e^{i\beta \hat{t}} \sum_{n=0}^{\infty} \left(e^{-\alpha \lambda_s} \frac{1}{n!} \left[\alpha \int_{-\infty}^{\infty} P(\beta') e^{-\beta'/2} e^{-i\beta' \hat{t}} \, d\beta' \right]^n \right) \, d\hat{t} \tag{1.13}$$

$$= e^{-\alpha \lambda_s} \sum_{n=0}^{\infty} \frac{\alpha^n}{n!} \frac{1}{2\pi} \int_{-\infty}^{\infty} e^{i\beta \hat{t}} \left[\int_{-\infty}^{\infty} P(\beta') e^{-\beta'/2} e^{-i\beta' \hat{t}} \, d\beta' \right]^n \, d\hat{t} \tag{1.14}$$

$$= e^{-\alpha \lambda_s} \sum_{n=0}^{\infty} \frac{1}{n!} \left[\alpha \lambda_s \right]^n \mathcal{T}_n(\beta) \tag{1.15}$$

where

$$\lambda_s^n \mathcal{T}_n(\beta) = \frac{1}{2\pi} \int_{-\infty}^{\infty} e^{i\beta \hat{t}} \left[\int_{-\infty}^{\infty} P(\beta') e^{-\beta'/2} e^{-i\beta' \hat{t}} \, d\beta' \right]^n \, d\hat{t}. \tag{1.16}$$

Note that

$$\mathcal{T}_0(\beta) = \delta(\beta) \tag{1.17}$$

and

$$\mathcal{T}_1(\beta) = \frac{1}{2\pi\lambda_s} \int_{-\infty}^{\infty} e^{i\beta\hat{t}} \int_{-\infty}^{\infty} P(\beta')e^{-\beta'/2}e^{-i\beta'\hat{t}} \, d\beta' \, d\hat{t} \qquad (1.18)$$

$$= \frac{1}{2\pi\lambda_s} \int_{-\infty}^{\infty} P(\beta')e^{-\beta'/2} \int_{-\infty}^{\infty} e^{i(\beta-\beta')\hat{t}} \, d\hat{t} \, d\beta' \qquad (1.19)$$

$$= \frac{1}{\lambda_s} \int_{-\infty}^{\infty} P(\beta')e^{-\beta'/2}\delta(\beta - \beta') \, d\beta' \qquad (1.20)$$

$$= \frac{P(\beta)e^{-\beta/2}}{\lambda_s}. \qquad (1.21)$$

As shown in Appendix A.1, $\mathcal{T}_n(\beta)$ can be attained using a convolution integral,

$$\mathcal{T}_n(\beta) = \int_{-\infty}^{\infty} \mathcal{T}_1\left(\beta'\right)\mathcal{T}_{n-1}\left(\beta - \beta'\right) d\beta'. \qquad (A.8)$$

Solving the solid-type, continuous contribution to $S_{n.sym}(\alpha, \beta, T)$ can be done by computing $\mathcal{T}_i(\beta)$ for i from 1 to a sufficiently large value of n. These $\mathcal{T}_i(\beta)$ values can be used in the Eq. 1.15, which directly contributes to $S_{n.sym}(\alpha, \beta, T)$.

Discrete Oscillator

Shown in Fig. 1.1 is the phonon distribution for H in H_2O, as calculated by [5]. Often,
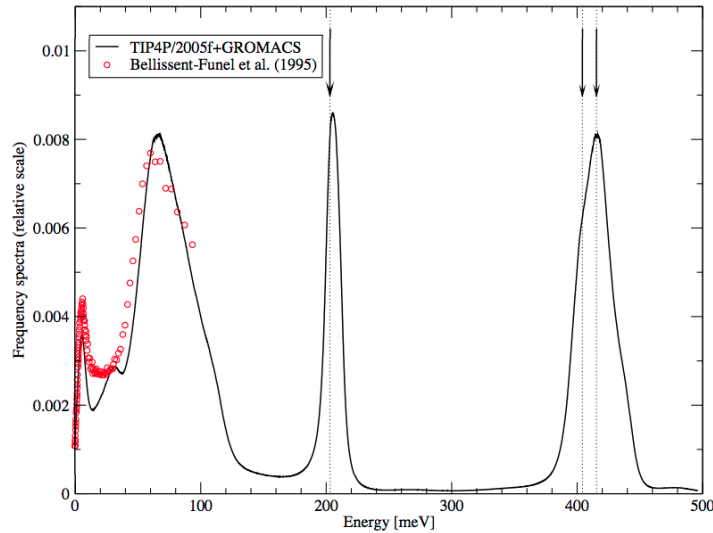

Figure 1.1: Phonon Distribution for H in H_2O [5]. The red points and the arrows represent measured data against which to compare the calculated spectrum. Of particular interest are the two peaks near 200 and 400 meV, which are approximated in LEAPR as discrete oscillators.

vibrational modes appear as sharp peaks in the frequency distribution, and can be treated

as a weighted delta functions, $\omega_i\delta_i(E)$. The contribution to the scattering law from oscillator i is

$$S_{n.sym}^{(i)}(\alpha,\beta) = e^{-\alpha\lambda_i} \sum_{n=-\infty}^{\infty} \delta\left(\beta - n\beta_i\right) I_n\left[\frac{\alpha w_i}{\beta_i \sinh\left(\beta_i/2\right)}\right] e^{-n\beta_i/2} \tag{1.22}$$

where the corresponding Debye-Waller coefficient is

$$\lambda_i = w_i \frac{\coth\left(\beta_i/2\right)}{\beta_i} \tag{1.23}$$

and $I_n(x)$ is the modified Bessel function of the first kind. When combining a continuous, solid-type spectrum with discrete oscillators, the total Debye-Waller coefficient is simply the sum,

$$\lambda = \lambda_s + \sum_{i=1}^{N} \lambda_i \tag{1.24}$$

where there are N oscilllators considered. Combining all the factors in Eq. 1.22 without a β term leaves us with

$$S_{n.sym}^{(i)}(\alpha,\beta) = \sum_{n=-\infty}^{\infty} A_{i,n}(\alpha)\delta\left(\beta - n\beta_i\right) \tag{1.25}$$

where $A_{i,n}(\alpha)$ is defined as

$$A_{i,n}(\alpha) = e^{-\alpha\lambda_i} I_n\left[\frac{\alpha\omega_i}{\beta_i \sinh(\beta_i/2)}\right] e^{-n\beta_i/2}. \tag{1.26}$$

Using Eq. 1.22 or Eq. 1.25, the contribution that an individual oscillator has to the total scattering law is rather simple to compute. Once computed, it must be convoled with the existing scattering law. Consider an example where two discrete oscillators contributions, $S_{n.sym}^{(1)}$ and $S_{n.sym}^{(2)}$, are being combined to a scattering law contribution from solid type spectrum $S_{n.sym}^{(s)}$.

$$S_{n.sym}^{(s,1)}(\alpha,\beta) = \int_{-\infty}^{\infty} S_{n.sym}^{(1)}\left(\alpha,\beta'\right) S_{n.sym}^{(s)}\left(\alpha,\beta - \beta'\right) d\beta' \tag{1.27}$$

$$= \int_{-\infty}^{\infty} \sum_{n=-\infty}^{\infty} A_{1,n}(\alpha)\delta\left(\beta' - \beta_1\right) S_{n.sym}^{(s)}\left(\alpha,\beta - n\beta'\right) d\beta' \tag{1.28}$$

$$= \sum_{n=-\infty}^{\infty} A_{1,n}(\alpha) S_{n.sym}^{(s)}\left(\alpha,\beta - n\beta_1\right) \tag{1.29}$$

$$S_{n.sym}^{(s,1,2)}(\alpha, \beta) = \int_{-\infty}^{\infty} S_{n.sym}^{(2)}(\alpha, \beta') \, S_{n.sym}^{(s,1)}(\alpha, \beta - \beta') \, d\beta' \tag{1.30}$$

$$= \int_{-\infty}^{\infty} \sum_{m=-\infty}^{\infty} A_{2,m}(\alpha) \delta \left(\beta' - m\beta_2 \right) S_{n.sym}^{(s,1)}(\alpha, \beta - \beta') \, d\beta' \tag{1.31}$$

$$= \sum_{m=-\infty}^{\infty} A_{2,m}(\alpha) S_{n.sym}^{(s,1)}(\alpha, \beta - m\beta_2) \tag{1.32}$$

$$= \sum_{m=-\infty}^{\infty} A_{2,m}(\alpha) \sum_{n=-\infty}^{\infty} A_{1,n}(\alpha) S_{n.sym}^{(s)}(\alpha, \beta - n\beta_1 - m\beta_2) \tag{1.33}$$

$$\tag{1.34}$$

Translational Spectra

Thermal neutron scattering off of some materials, especially gasses and liquids, can be modeled by considering a solid-type, continuous spectrum, combined with a diffusive term. For liquid moderators, LEAPR makes use of the "effective width model" [6]. The effective width model defines the translational contribution to the scattering law as

$$S_{n.sym}^{(t)}(\alpha, \beta) = e^{[2c^2 w_t \alpha - \beta/2]} \frac{2cw_t \alpha \sqrt{c^2 + .25}}{\pi \sqrt{\beta^2 + 4c^2 w_t^2 \alpha^2}} K_1 \left\{ \sqrt{c^2 + .25} \sqrt{\beta^2 + 4c^2 w_t^2 \alpha^2} \right\} \tag{1.35}$$

with the phonon distribution is defined as

$$\rho(\beta) = w_t \frac{4c}{\pi\beta} \sqrt{c^2 + .25} \sinh(\beta/2) K_1 \left\{ \sqrt{c^2 + .25} \beta \right\} \tag{1.36}$$

where w_t is the translational weight, c is the diffusion constant, and K_1 is the modified Bessel function of the second kind.

For gas moderators, and even some liquid moderators, the free gas approximation can be used as an alternative to the effective width model,

$$S_{n.sym}^{(t)}(\alpha, \beta) = e^{-\beta} \frac{1}{\sqrt{4\pi w_t \alpha}} \exp \left[-\frac{(w_t \alpha - \beta)^2}{4w_t \alpha} \right]. \tag{1.37}$$

Once the translational contribution to the scattering law is calculated, it is convolved with the other contributions to obtain the total $S_{n.sym}(\alpha, \beta)$.

1.3 Areas of Improvement

1.3.1 Input Phonon Distribution Approximations

1.3.2 Sampling from $S(\alpha, \beta, T)$

Chapter 2

Accurate Representation of Phonon Distributions

2.1 Discrete Oscillator Approximation

The LEAPR module of NJOY, which is used to prepare thermal scattering data in the form of the scattering law, $S(\alpha, \beta, T)$, often approximates peaks in the phonon spectra as discrete oscillators, and models them as weighted δ-functions. In the event that a user would want to avoid this approximation, and instead apply the continuous phonon distribution treatment to those selected areas, it is crucial to verify agreement between these two methods. To test this, a simplified version of the NJOY 2016 release Test Problem 9 is considered [3]. The LEAPR component of Test Problem 9 models H in H_2O using a slightly simplified phonon spectrum, and moderately coarse α, β grids (65 and 75 values, respectively). Fig. 2.1 contains the phonon spectrum that NJOY 2016 uses in their Test Problem 9.

For Test Problem 9, the continuous region of phonon is defined as $\rho(\beta) = \rho(\Delta E / k_b T)$ for ΔE spanning from 0-0.16575 eV, where the energy grid is uniformly spaced in increments of 0.00255 eV. The translational contribution to Test Problem 9 is removed ($\omega_t = 0$), and thus the continuous weighting (ω_s) is increased from 0.444444 to 0.5. The locations and weights of the two discrete oscillators are provided in Table 2.1. Note that, as required by Eq.1.9,

$$\omega_s + \omega_1 + \omega_2 = 0.5 + 0.166667 + 0.333333 = 1.0. \tag{2.1}$$

Table 2.1: Energies and Weights for δ functions used in NJOY 2016 Test Problem 9

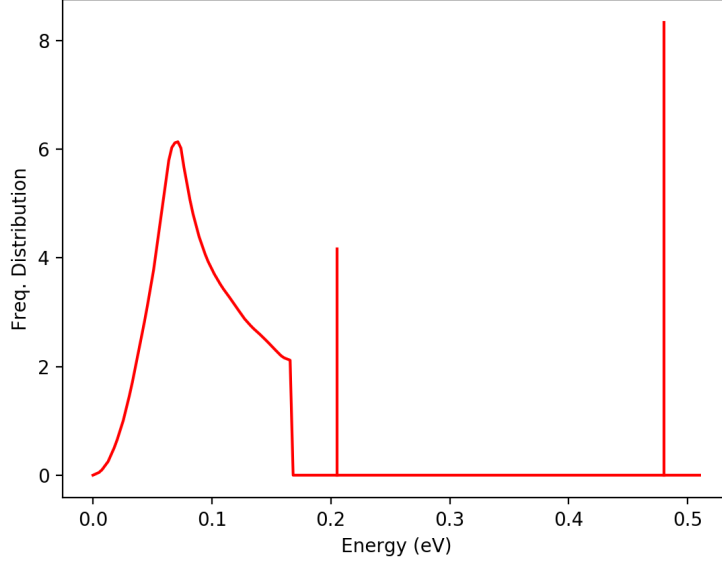| Energy (eV)	Weighting
0.205	0.166667
0.480	0.333333

Figure 2.1: The phonon distribution for NJOY 2016 Test Problem 9 is shown above. It contains a continuous contribution, shown on the lower energy region, and two δ functions to approximate the higher energy peaks.

2.2 Representing Discrete Oscillators as Continuous Points in Freq. Dist.

In order to allow users to avoid the δ function approximation that is commonly used in NJOY's LEAPR module, it is crucial to demonstrate similar behavior between how the solid-type, continuous treatment vs. discrete oscillator treatment processes sharp peaks. For this discussion, Test Problem 9, which was described in Sec. 2.1 is considered. To allow for more flexible analysis, LEAPR's source code was translated from Fortran to C++. So first, the results of the translated C++ LEAPR are compared against legacy Fortran LEAPR for the simple H in H_2O model, to establish valididty in the method. Then, the discrete oscillators in Test Problem 9 are replaced with triangles of varying thickness, to illustrate that as the thickness of the triangle decreases, it approaches the behavior characteristic of a δ function oscillator.

2.2.1 Equivalence of Revised-LEAPR to Legacy-LEAPR

NJOY's LEAPR module was translated from Fortran to C++, so as to provide flexibility in later analysis. The C++ translation must of course replicate the original NJOY code adequately. To illustate this, Fig. 2.2 contains $S(\alpha, \beta)$ as it was calculated using both the original LEAPR code, as well as the translated LEAPR code. Note that the for nearly all α, β values shown, the two datasets are virtually indistinguishable from each other.
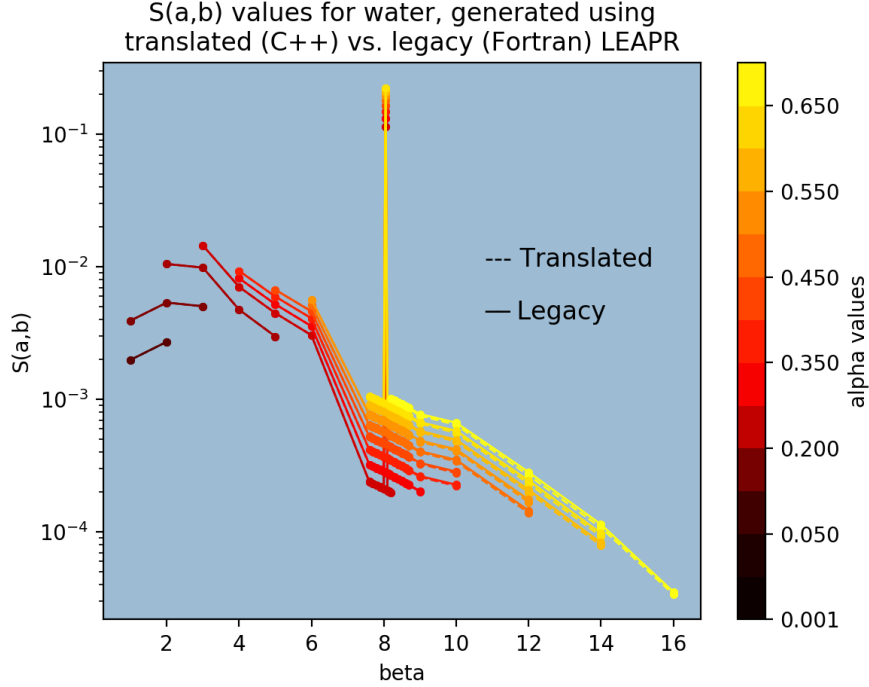
Figure 2.2: Comparison of $S(\alpha, \beta)$ results, comparing translated (C++) vs. legacy (Fortran) LEAPR for H in H$_2$O Test #9 Input. The translated- and legacy-generated results are represented with dotted and solid lines, respectively.

Fig. 2.3 shows the percent error between the $S(\alpha, \beta)$ values produced by the translated and original LEAPR, that were plotted in Fig. 2.2. Notice that the percent error is significantly lower in the β regions where $S(\alpha, \beta)$ is of reasonable size.

Thus, the translated version of LEAPR is considered an adequate tool for processing thermal data for the following discussion. However, conclusions drawn using the translated LEAPR will be verified alongside those drawn from the legacy LEAPR. Note that the translated LEAPR was also tested against legacy LEAPR with other cases considered.

2.2.2 Replacing Discrete Oscillator δ Functions as Triangles

To verify that discrete oscillator treatment can be replicated by using increasingly thin triangles, each triangle must integrate to the weight of its corresponding δ function. Triangles of various widths (2,4,6,8, and 10 grid spaces) are used to replace both δ functions, and are plotted in Fig. 2.4.

NJOY requires any continuous phonon distribution to be provided with respect to a uniformly-spaced energy grid. Thus, in Fig. 2.4, the centers of the triangles are not necessarily equal to the exact location of the δ functions that are specified in Table. 2.1. A closer view of Fig. 2.4, shown in Fig. 2.5, illustrates an offset between the triangle centers and the real oscillator location. Since the triangles' points are limited to increments of $\Delta E = 0.00255$ eV, some inaccuracies are to be expected.
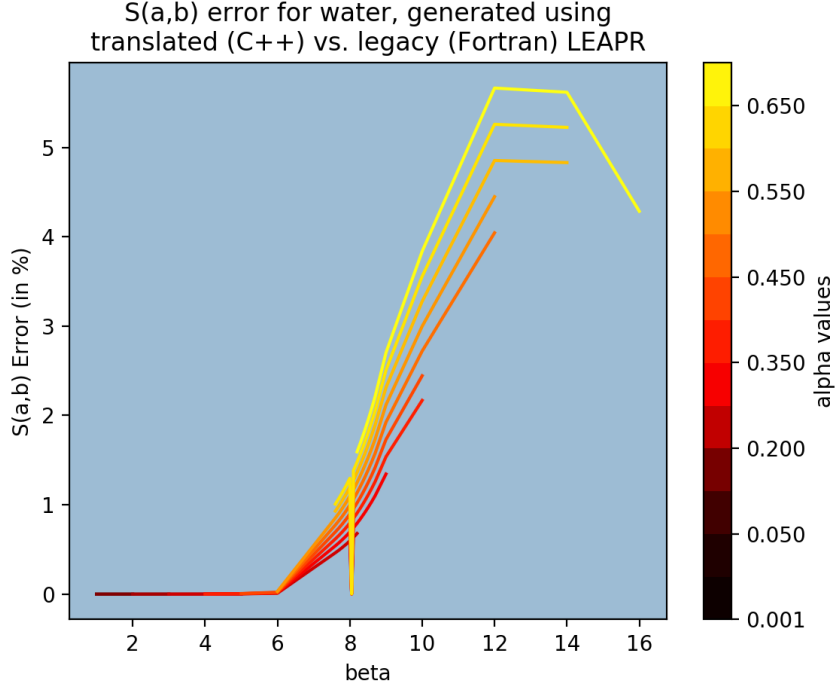
18

Figure 2.3: Comparison of translated vs. legacy LEAPR, for test #9, with the percent error plotted. Note that in the β region where percent error increases, is the same region in Fig. 2.2 where the $S(\alpha, \beta)$ values become significantly smaller.

Table 2.2: Energies and Weights for δ functions, Amended to Align with Continuous Energy Grid

Energy (eV)	Weighting
0.204	0.166667
0.4794	0.333333

As a result of the discrepancy between discrete oscillator location and triangle center location, the oscillators energies are shifted slightly to align better with the $\Delta E = 0.00255$ eV grid to which NJOY is restricted. The δ function parameters presented in Table. 2.1 are amended to those in Table. 2.2
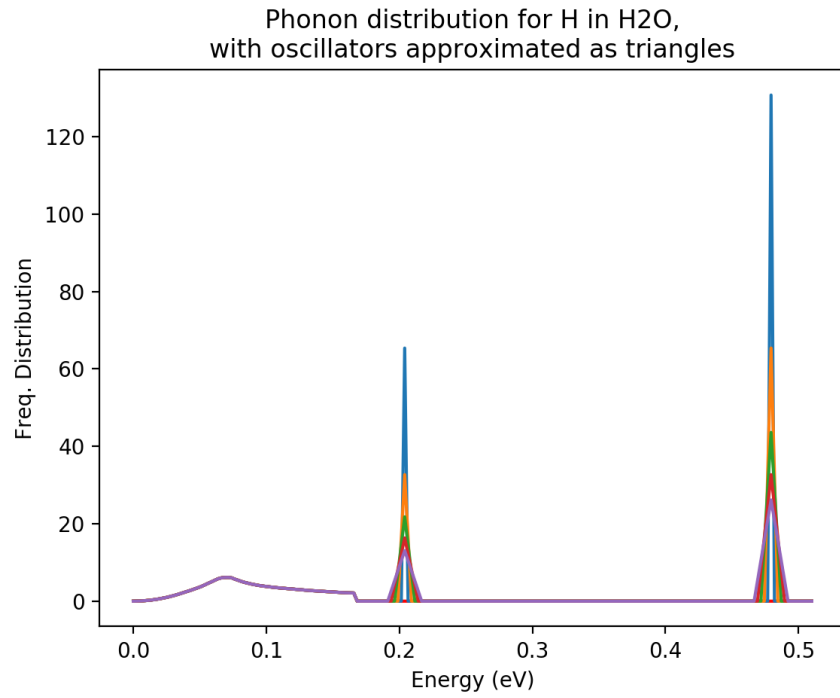
Figure 2.4: Phonon Distribution for H in H_2O, with oscillators replaced with phonon distribution triangles of various widths. The area under each triangle integrates to its corresponding δ function weight ω_i, and the lower energy continuous component integrates to the solid-type weight ω_s.
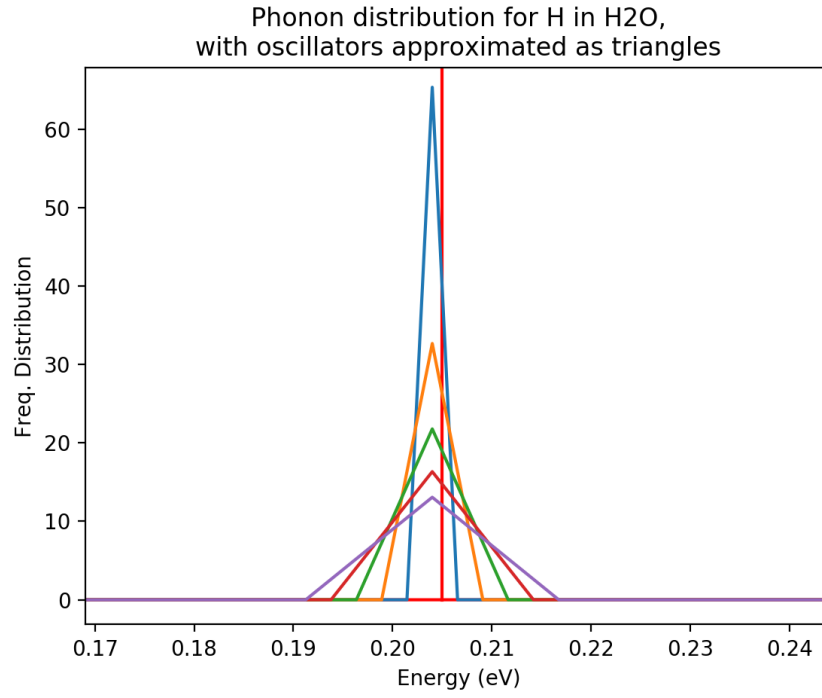
Figure 2.5: This is a zoomed in version of Fig. 2.4, where we focus in on the 0.204 eV δ function. The red line represents the δ function that is defined in the test #9, while other colors represent triangles used to approximate the δ function.

2.2.3 $S(\alpha, \beta)$ Response to Changes in Triangle Size

This is where I want to pick a few α values, and show how changing triangle size affects $S(\alpha, \beta)$

2.3   Nonuniform Phonon Distribution Energy Grid

Identifying the effect that changing δ functions to triangles has on $S(\alpha, \beta)$, for H in H_2O

Problem Specification

We approximate the delta functions to be triangles of various widths. This is shown in Fig. 2.4. The continuous description spans from 0 eV to 0.17 eV.

Results: Thin Triangle vs. δ Func.

We use the phonon distributions generated earlier as input for NJOY, and generate resultant $S(\alpha, \beta)$ grids. We consider a phonon distribution with δ functions describing the higher energy region (with the energies and weights that are presented in Table 2), alongside a phonon distribution with thin triangles approximating the δ functions. The triangles used to approximate the δ functions have a total width of two spaces, or $2 \times 0.00255 = 0.0051$ eV.
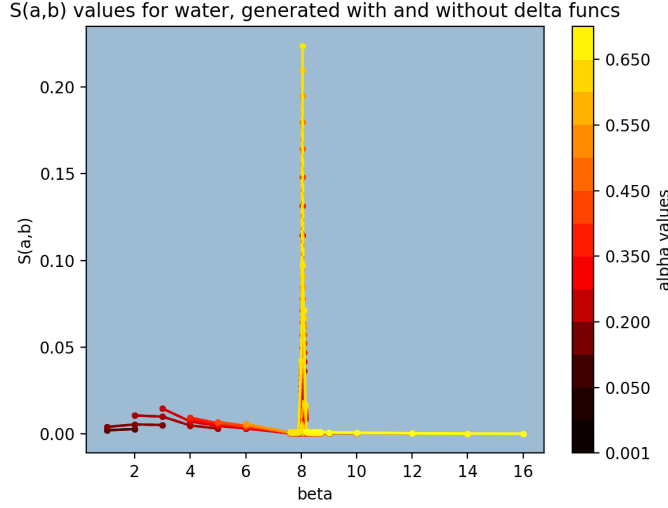

Figure 2.6: NJOY is used to generate the above plots, where we plot $S(\alpha, \beta)$ against β, for various α values. Note that since not all α values are compatible with all β values, we have discrete line sort of behavior, especially for the low β region.

Let's look at Fig. 2.7, which is a zoomed-in version of Fig. 2.6. It shows the $S(\alpha, \beta)$ values that were generated using NJOY for H in H_2O, wusing the δ function phonon distribution (dotted lines) and the triangle approximation to δ functions (solid lines). Note that $S(\alpha, \beta)$ grid that uses the triangle approximation for its higher energy peaks has more of a smear than the one that uses δ functions, which seems pretty reasonable.

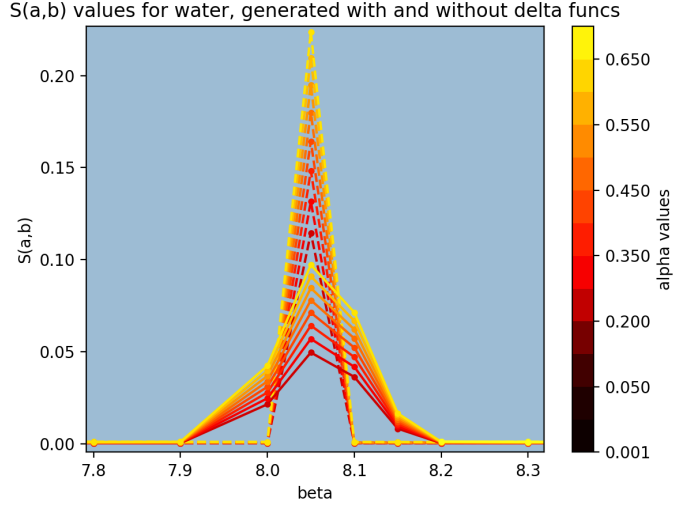S(a,b) values for water, generated with and without delta funcs

Figure 2.7: This is the same as Fig. 2.6, except we zoom in on the peak near $\beta \approx 8.05$. The dotted lines correspond to the values produced by NJOY using δ functions in the phonon distribution, while the solid lines correspond to those δ functions being approximated by a thin triangle.

Results: Triangles of Various Widths vs. δ Func.

We also look at the total error.

$$E_{total} = \sum_{\beta} \sum_{\alpha} \left| S^{\delta}(\alpha, \beta) - S^{\triangleleft}(\alpha, \beta) \right|$$
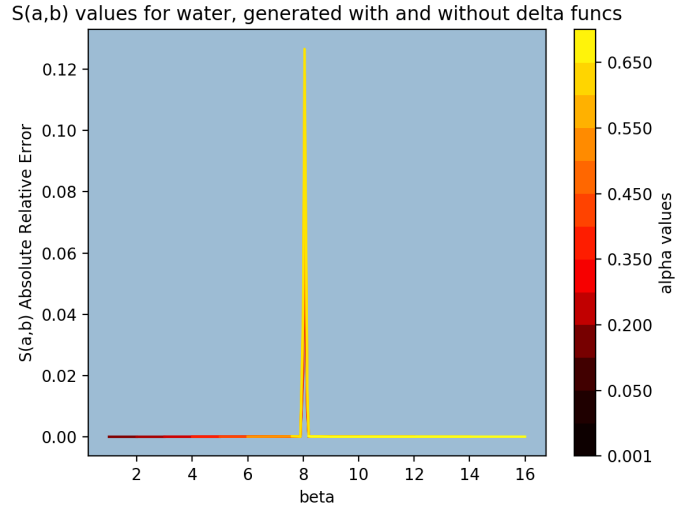
Figure 2.8: This is the absolute relative error between the $S(\alpha, \beta)$ produced using δ functions and $S(\alpha, \beta)$ produced using a thin (width = 2 spaces) triangle. Note that the error is very small away from the $\beta \approx 8.05$ peak.
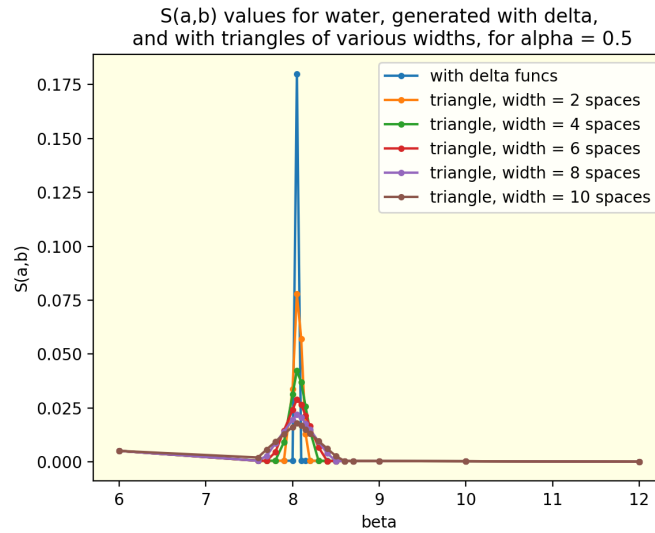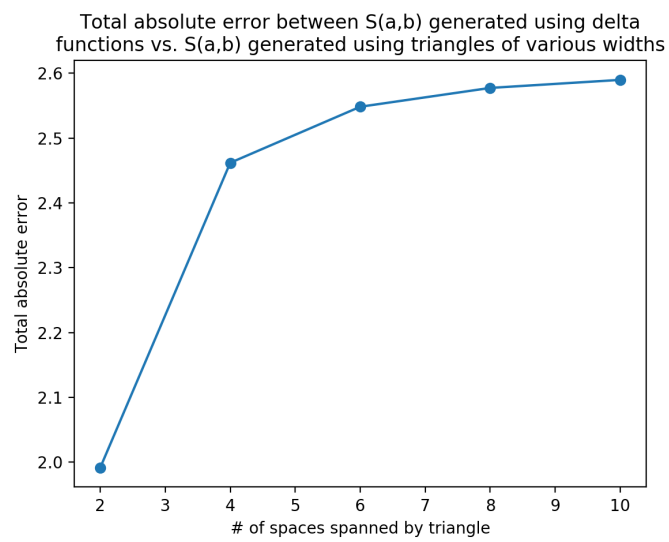

Figure 2.9:

Figure 2.10: Note that as the width of the triangle decreases, the total accumulated error decreases significantly.

Chapter 3

Improved Sampling of $S(\alpha, \beta)$

This is where I'm going to talk about Pavlou's paper

Bibliography

[1]   M Herman, Cross Sections Evaluation Working Group, et al. *ENDF-6 Formats Manual Data Formats and Procedures for the Evaluated Nuclear Data File ENDF/B-VI and ENDF/B-VII*. Tech. rep. Brookhaven National Laboratory (BNL) National Nuclear Data Center, 2009.

[2]   *ADS Nuclear Data Library. ACE formatted Library for Accelerator Driven Systems*. https://www-nds.iaea.org/adsV1/adsace.html. [Online; accessed 7-December-2017]. 2005.

[3]   Robert Macfarlane et al. *The NJOY Nuclear Data Processing System, Version 2016*. Tech. rep. Los Alamos National Laboratory (LANL), 2017.

[4]   Jesse Curtis Holmes. "Monte Carlo Calculation of Thermal Neutron Inelastic Scattering Cross Section Uncertainties by Sampling Perturbed Phonon Spectra". PhD thesis. North Carolina State University, 2014.

[5]   JI Marquez Damian, JR Granada, and DC Malaspina. *CAB models for water: a new evaluation of the thermal neutron scattering laws for light and heavy water in ENDF-6 format*. Tech. rep. 2014, pp. 280–289.

[6]   PA Egelstaff and P Schofield. "On the evaluation of the thermal neutron scattering law". In: *Nuclear Science and Engineering* 12.2 (1962), pp. 260–270.

Appendices

Appendix A

Background

A.1 $T_n(\beta)$ Representation as a Convolution Integral

$$\mathcal{T}_n(\beta) = \frac{1}{2\pi} \frac{1}{\lambda_s^n} \int_{-\infty}^{\infty} \mathrm{e}^{i\beta\hat{t}} \left[\int_{-\infty}^{\infty} P(\beta') \mathrm{e}^{-\beta'/2} \mathrm{e}^{-i\beta'\hat{t}} \, d\beta' \right]^n \, d\hat{t}. \tag{A.1}$$

$$\mathcal{T}_n(\beta) = \frac{1}{2\pi} \frac{1}{\lambda_s^n} \int_{-\infty}^{\infty} \mathrm{e}^{-i\beta\hat{t}} \left[\int_{-\infty}^{\infty} P(\beta') \mathrm{e}^{\beta'/2} \mathrm{e}^{-i\beta'\hat{t}} \, d\beta' \right] \left[\int_{-\infty}^{\infty} P(\beta'') \mathrm{e}^{-\beta''/2} \mathrm{e}^{-i\beta''\hat{t}} \, d\beta'' \right]^{n-1} \, d\hat{t} \tag{A.2}$$

$$\mathcal{T}_n(\beta) = \frac{1}{2\pi} \frac{1}{\lambda_s^n} \int_{-\infty}^{\infty} \int_{-\infty}^{\infty} \mathrm{e}^{-i\beta\hat{t}} P(\beta') \mathrm{e}^{\beta'/2} \mathrm{e}^{-i\beta'\hat{t}} \left[\int_{-\infty}^{\infty} P(\beta'') \mathrm{e}^{-\beta''/2} \mathrm{e}^{-i\beta''\hat{t}} \, d\beta'' \right]^{n-1} \, d\beta' \, d\hat{t} \tag{A.3}$$

$$\mathcal{T}_n(\beta) = \frac{1}{2\pi} \frac{1}{\lambda_s^n} \int_{-\infty}^{\infty} \mathrm{e}^{-i\beta\hat{t}} P(\beta') \mathrm{e}^{\beta'/2} \int_{-\infty}^{\infty} \mathrm{e}^{-i\beta'\hat{t}} \left[\int_{-\infty}^{\infty} P(\beta'') \mathrm{e}^{-\beta''/2} \mathrm{e}^{-i\beta''\hat{t}} \, d\beta'' \right]^{n-1} \, d\hat{t} \, d\beta' \tag{A.4}$$

$$\mathcal{T}_n(\beta) = \frac{1}{2\pi} \frac{1}{\lambda_s^n} \int_{-\infty}^{\infty} P(\beta') \mathrm{e}^{\beta'/2} \left[\int_{-\infty}^{\infty} \mathrm{e}^{i(\beta-\beta')\hat{t}} \left[\int_{-\infty}^{\infty} P(\beta'') \mathrm{e}^{-\beta''/2} \mathrm{e}^{-i\beta''\hat{t}} \, d\beta'' \right]^{n-1} \, d\hat{t} \right] d\beta' \tag{A.5}$$

$$\mathcal{T}_n(\beta) = \int_{-\infty}^{\infty} \frac{P(\beta') \mathrm{e}^{\beta'/2}}{\lambda_s} \left[\frac{1}{2\pi \lambda_s^{n-1}} \int_{-\infty}^{\infty} \mathrm{e}^{i(\beta-\beta')\hat{t}} \left[\int_{-\infty}^{\infty} P(\beta'') \mathrm{e}^{-\beta''/2} \mathrm{e}^{-i\beta''\hat{t}} \, d\beta'' \right]^{n-1} \, d\hat{t} \right] d\beta' \tag{A.6}$$

$$\mathcal{T}_n(\beta) = \int_{-\infty}^{\infty} \frac{P(\beta') \mathrm{e}^{\beta'/2}}{\lambda_s} \mathcal{T}_{n-1}\left(\beta - \beta'\right) d\beta' \tag{A.7}$$

$$\mathcal{T}_n(\beta) = \int_{-\infty}^{\infty} \mathcal{T}_1\left(\beta'\right) \mathcal{T}_{n-1}\left(\beta - \beta'\right) d\beta' \tag{A.8}$$